Computational Studies of Non-Equilibrium Molecular Transport through Carbon Nanotubes

Ki-Ho Lee and Susan B. Sinnott*

Department of Materials Science and Engineering, University of Florida, Gainesville, Florida 32611-6400

Received: September 18, 2003; In Final Form: May 6, 2004

The transport of methane molecules into several open-ended carbon nanotubes is studied with classical, nonequilibrium molecular dynamics simulations. The forces in the simulations are determined using a reactive empirical bond order potential for short-ranged interactions and a Lennard-Jones potential for long-range interactions. The simulations show that until the carbon nanotubes are filled with methane molecules up to a specific cutoff molecular density, the molecules move forward and backward along the axis of nanotubes in a "bouncing" motion. This bouncing motion is observed for molecules inside both hydrogen-terminated and non-hydrogen-terminated opened nanotubes and is caused by a conflict between the molecules' attractive interactions with the interior of the nanotube and their response to the molecular density gradient down the length of the tube. At molecular densities above the cutoff value, the molecules flow into, through, and out of the nanotubes in a linear manner. The effects of molecular density, nanotube diameter, and nanotube helical symmetry on the results are analyzed.

1. Introduction

The flow of small gas or liquid molecules through porous materials is of great interest to the chemical and pharmaceutical industries. Research has primarily focused on the study of molecular transport through macroporous and microporous systems, but in recent years the study of fluid flow through nanopores has been encouraged by the discovery and development of nanoporous materials such as zeolites and carbon nanotubes.[1−4] Some of these materials have found industrial application in the adsorption, separation, or promotion of catalytic processes in multicomponent fluids.[5,6] However, the mechanism for flow, diffusion, adsorption, and separation of multicomponent molecular mixtures in nanoporous materials is difficult to study experimentally. This is in part because it is nontrivial to prepare self-supporting nanoporous materials with uniform pore sizes and distributions on the order of 1−100 nm. It is also difficult to detect and trace the behavior of molecules inside nanopores. Therefore, computational methods, such as molecular dynamics (MD) or Monte Carlo (MC) simulations have been widely used as an alternative to determine these mechanisms in zeolites and ideal nanopores.[7,8]

Computational studies thus play an important role in the analysis of experimental data and provide predictive information about molecular mass-transport through nanopores. Atomistic computational studies have shown that the diffusion properties of molecules confined in nanometer-scale spaces are very different from those of bulk fluids that are well described by continuum theory. Commonly known diffusion mechanisms include normal-mode diffusion, where molecules are able to pass each other;[9] single-file diffusion, where molecules are unable to pass each other;[10,11] and a mode that is between these two that is called transition-mode diffusion.[12]

Numerous groups have studied the diffusion of molecules in zeolites by computational methods,[10,13−17] and shown that molecular diffusion modes depend significantly on the types of molecules involved; that is, larger molecules usually diffuse by single-file mode, and smaller molecules tend to diffuse by normal-mode diffusion. In other studies on the separation of molecular mixtures, such as methane/*n*-butane mixtures, their behavior in silicate nanopores has been examined by quasielastic neutron scattering experiments and MD simulations, which indicate that the nanopore can separate the mixture.[18]

Carbon nanotubes are similar to zeolites in that they contain nanometer-scale pores, but they may induce different fluid dynamics than other molecular sieves. This is because nanotubes have continuous, smooth walls of uniform composition, whereas zeolites generally have nonuniformly distributed sizes of diameters and are composed of multiple elements. In addition, variations in the helical alignment of carbon atoms along the nanotube axis may influence molecular motion. The flow of *n*-pentane and isopentane molecules through carbon nanotubes is predicted to show a different kind of motion from the flow of these molecules in zeolites.[19] Additionally, the self-diffusivities and transport diffusivities of Ar and Ne in carbon nanotubes are predicted to be larger by, at most, 3 orders of magnitude relative to flow in silicates.[20] These studies illustrate the way in which the identity of the nanoporous material affects molecular diffusive flow.

Several groups have studied the influx of numerous compounds inside carbon nanotubes in experiments,[21−23] first principles calculations for HF molecular flow into small carbon nanotubes,[24] hydrogen adsorption in nanotubes bundles,[25−27] and the dynamic flow of helium and argon atoms through nanotubes.[28] Numerous computational studies have also considered the intercalation of small molecules and noble gas atoms, such as hydrogen, nitrogen, and helium, into opened single-walled nanotubes or the interstitial sites between the nanotubes in a

* Author to whom correspondence should be addressed. E-mail: sinnott@mse.ufl.edu.

10.1021/jp036791j CCC: $27.50
Published on Web 06/17/2004

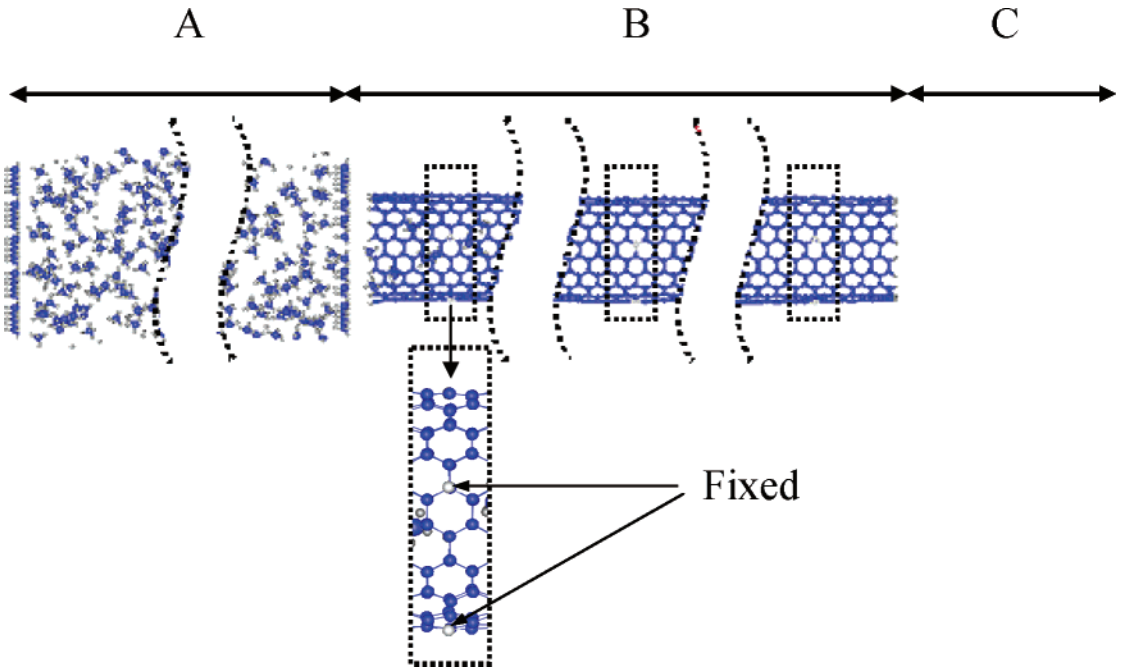

Figure 1. Snapshot of the simulation model. CH_4 molecules are flowing into a (10,10) nanotube. Region A is a gas reservoir, region B is a nanotube region, and region C is a posterior region.

bundle.[29−37] Larger molecules and noble gas atoms, such as xenon, methane, and neon, are also predicted to diffuse into nanotubes.[37−39] The transport of water molecules, which form strong intermolecular interactions in a carbon nanotube, has been studied in simulations by Hummer et al.[40,41] Experimentally, it has also been determined that methane molecules can diffuse into single-walled nanotubes with a diffusion coefficient between 3×10^{-7} and 15×10^{-7} cm^2/s at about 90 K.[42]

Previous MD simulations by one of us predicted that transition-mode diffusion in carbon nanotubes and bundles occurs primarily with nonspherical molecules such as ethane but does not occur for spherical molecules such as methane.[43,44] The separation of molecular mixtures via dynamic diffusion through individual, single-walled carbon nanotubes and through nanotubes in bundles was also considered.[44] Here we extend our MD study of methane transport for longer time periods and through longer, hydrogen-terminated carbon nanotubes than were considered previously. New molecular motions associated with the various stages of nonequilibrium transport of methane not previously seen are predicted to occur. In this paper, we characterize and discuss this new, nonequilibrium transport motion through carbon nanotubes.

2. Computational Details

The computational approach used in this research is classical MD simulations, where Newton's equations of motions are numerically integrated with a third-order Nordsieck predictor corrector integration algorithm to track the motion of the atoms with time. The time step used for the integration is 0.2 fs in all the simulations. The forces on the atoms are calculated using methods that vary with distance: short-range interactions are calculated using the second generation of the reactive, empirical bonding-order (REBO) hydrocarbon potential[45] that realistically describes covalent bonding within both the methane molecules and the carbon nanotubes. It has previously been used in combination with Lennard-Jones (LJ) potentials to study the diffusion of organic molecules and molecular mixtures through carbon nanotubes and nanotubes bundles.[43,44] In this work the long-range interactions are similarly characterized with a LJ potential.

The combined expression used to calculate the energy of the system in each case can therefore be expressed as follows:

$$U = \sum_i \sum_{i<j} [V_R(r_{ij}) - B_{ij} V_A(r_{ij}) + V_{vdw}(r_{ij})] \qquad (1)$$

where U is the binding energy, r_{ij} is the distance between atoms i and j, V_R is a pair-additive term that models the interatomic core−core repulsive interactions, and V_A is a pair-additive term that models the attractive interactions due to the valence electrons. In addition, B_{ij} is a many-body empirical bond-order term that modulates valence electron densities and depends on atomic coordination and bond angles. Detailed forms of these expressions can be found in ref 45. Finally, V_{vdw} is the LJ potential, shown in eq 2, that models the van der Waals interactions, and is only nonzero after the short-range, REBO potential goes to zero.

$$V_{LJ} = 4\epsilon_{AB}\left[\left(\frac{\sigma_{AB}}{r_{ij}}\right)^{12} - \left(\frac{\sigma_{AB}}{r_{ij}}\right)^{6}\right] \qquad (2)$$

In eq 2, ϵ_{AB} and σ_{AB} are LJ empirical parameters for the interaction between A and B. The van der Waals interaction is minimized at an interatomic distance of $\sqrt[6]{2}\sigma$, which is 2.56 Å for C−C and is 2.86 Å for C−H. At every time step, the forces are determined using

$$F_{ij,k} = -\left(\frac{\partial U}{\partial r_{ij,k}}\right) \qquad (3)$$

where k denotes a coordinate direction, F_{ij} is the force between particles i and j, and r_{ij} is the distance between particles i and j.

The system setup is shown in Figure 1. Within the figure, Region A is the gas reservoir, region B contains the nanotube, and region C is called the posterior region. Periodic boundary conditions[46] are applied to the system in the directions perpendicular to the nanotube axis. To maintain the system temperature at 300 K, a Langevin thermostat[47] is applied to the nanotube walls throughout the simulations and to both the nanotube walls

TABLE 1: Properties of the Carbon Nanotubes Considered

helicity	type	radius (Å)	length (Å)	number of C/H atoms
10,0	zigzag	3.97	106.58	980/20
14,0	zigzag	5.56	106.58	1372/28
17,0	zigzag	6.75	106.58	1666/34
6,6	armchair	4.12	109.13	1044/24
8,8	armchair	5.50	109.13	1392/32
10,10	armchair	6.88	109.13	1740/40

and region A during system equilibration. The molecules are initially distributed on a grid and separated from each other by distances appropriate for van der Waals interactions at room temperature. The entire system is then equilibrated for 800 fs prior to the start of transport.

The gas reservoir is built to model methane at a density 0.273 g/cm^3 (750 molecules) at 300 K and 500 atm.[48] The CH_4 molecules in region A are separated from the nanotube opening by 2.5 to 2.8 Å. To keep the CH_4 molecules from moving away from the nanotube, a "wall" of CH_4 molecules at the far end of region A and at the interface between regions A and B (excluding an opening that corresponds to the location of the nanotube opening) are held fixed and are not allowed to evolve during the simulations. This keeps the gas molecules within region A so that their only way out of the gas reservoir in through the opened carbon nanotube. It also maintains a molecular density gradient across the length of the nanotube.

Several different nanotubes with armchair or zigzag chiralities[49] are considered in region B. Table 1 shows the specifications of the nanotubes used in the simulations. In all cases, both ends of the nanotubes are open and terminated with hydrogen atoms. To prevent the whole rotation or translation of the carbon nanotube over the course of each simulation, eight atoms at about 10 Å from the tips and four atoms in the middle of each nanotube are held fixed as shown in Figure 1. All the remaining nanotube atoms are allowed to evolve but have Langevin thermostats applied to them to mimic the temperature-dissipation properties of a much longer nanotube and maintain the system's temperature at 300 K.

3. Results and Discussion

3.1. Characterization of Molecular Transport. In our previous studies[43,44,50] of CH_4 transport down 80 Å nanotubes for 100 ps, it was predicted that methane flowed into opened nanotubes and moved down their length from areas of high density to areas of low density following normal-mode diffusion:

$$\langle z^2 \rangle = 2At \tag{4}$$

where $\langle z^2 \rangle$ is the average square displacement that the molecules move, A is the diffusion coefficient, and t is time. The diffusion coefficients were taken from the intercepts in plots of the log of $\langle z^2 \rangle$ versus the log of t.

In the current study, the transport of the CH_4 molecules down tubes that are about 100 Å for 400 ps can be classified into three stages. In the first stage, CH_4 molecules enter the nanotube in region B and move down its axis. To enter the nanotube, a molecule must have a larger net repulsive force between the gas molecule and the other gas molecules in the gas reservoir than a net repulsive force between the gas molecule and nanotube tip atoms, or have enough kinetic energy to allow decelerated molecules to keep going into the nanotube. This stage is dominated by nonequilibrium transport and the molecular density inside the nanotube (region B) is quite low. When the molecule reaches the nanotube end closest to region C,

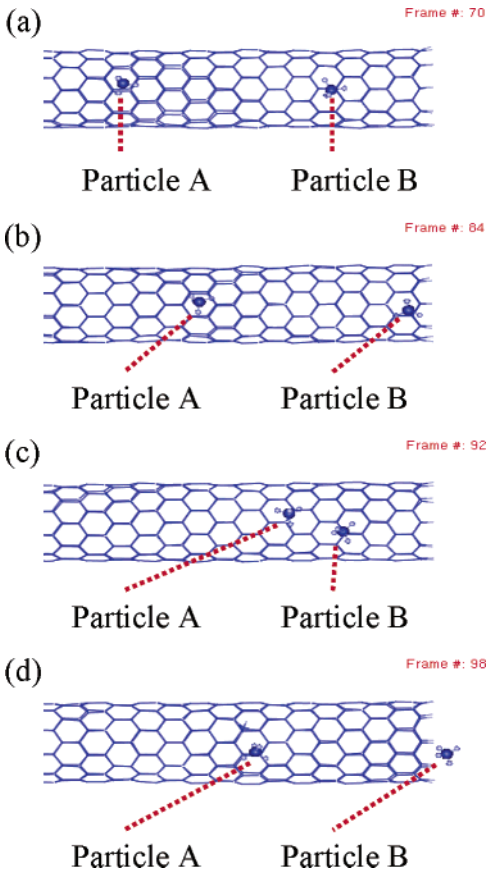

Figure 2. Snapshots of the rear side of region B (a) at 17.5 ps, (b) at 21 ps, (c) at 23 ps, and (d) at 24.5 ps. CH_4 molecules have entered the left end (not shown in the pictures) of a (10,0) nanotube.

depending on the kinetic energy of the molecule and the potential energy between the gas molecule and tip atoms of the nanotube, the molecule may or may not leave the nanotube. The molecule is affected by strong attractive van der Waals interactions with the nanotube atoms. As the diameter of the nanotube decreases, this attractive interaction increases because more nanotube tip atoms can get close to the molecule. The gas molecule that cannot overcome this attractive force changes its direction of motion and moves backward into the tube. Hence, at the end of the first stage, plots of log z versus log t do not have a linear relationship; instead, the data is scattered as the molecules move back and forth inside the nanotube.

The second stage of transport is dominated by chaotic flow, as some molecules move from region A to region B moving toward region C, and some molecules move from the interface between regions B and C and toward region A. The molecules moving forward and backward disturb the movements of the molecules that are just entering the nanotube by colliding with them, which initiates molecular "bouncing" motions inside the nanotube. As the simulation proceeds, the gas density in region B (inside the nanotube) increases, and the mean free path (average distance between collisions) of the gas molecules decreases. If the nanotube is longer, the period of the second stage is also longer. The carbon nanotubes used in this study are longer than those used in the previous studies. Therefore, the bouncing motion of the gas molecules, which had not been well observed in the previous studies, is clarified in these simulations. Figure 2 shows how the bouncing motion occurs at the side of region B closest to region C for the (10,0) nanotube system. The system is arranged in the same way as in Figure 1.

The right side of Figure 2 is the hydrogen-terminated nanotube and region C, while the left side of the picture is the middle of the nanotube. For clarity, only two methane molecules are shown. The direction of motion of the left-hand CH_4 is altered by a collision with the right-hand CH_4 (Figure 2b), and the direction of motion of the right-hand CH_4 is changed twice by an attractive interaction with the atoms at the end of the nanotube (Figure 2a) and by the collision with the left-hand CH_4 (Figure 2b).

As the simulation progresses, molecules continuously enter the nanotube from the gas reservoir moving toward the open end (region C). The buildup of molecular density in the nanotube overcomes the molecular attraction for the nanotube and forces molecules that are within the nanotube and near region C to exit. This is the third stage, which is characterized by near-steady-state transport of molecules from region A into the nanotube and out to region C. In this stage there is still some molecular motion in the opposite direction, from C to A, but it is much less dominant than it was in the second stage and the molecular motion is consequently significantly less chaotic.

Figure 3 shows plots of log $\langle z^2 \rangle$ versus log t for the initial 50 ps of simulation in the (10,0), (14,0), and (17,0) zigzag nanotubes, which corresponds to the first stage of molecular motion. Comparable behavior was seen for the similarly sized armchair (6,6), (8,8), and (10,10) nanotubes. The points labeled ASD denote the average square displacements of gas molecules through the nanotubes obtained from the simulations at the same periods starting when each sampled gas molecule enters the nanotube. The dotted ND I lines are fitted lines for the ASDs, assuming that these follow normal-mode diffusion behavior; dashed ND II lines are the normal-mode diffusion lines fit in our previous work.[43,44] The SD lines are fit to equations for anomalous transport, as discussed in detail below. The error bars are determined according to the following expression:

$$[\ln(\text{ASD} + \text{standard deviation}) - \ln(\text{ASD} - \text{standard deviation})]/2 \quad (5)$$

where the standard deviation is determined from the difference between the ASD and square displacement of each sampled molecule. The significant differences between ND I and ND II are attributed to statistics and several differences between the corresponding simulation systems and the analysis of the results. For example, in this study, ASD is determined for stage one by following various groups of 5 molecules for the initial 50 ps of transport down a 100 Å-long nanotube and averaging the results. The ND I line is then fit to these data. In contrast, the ND II line was initially fit by following one group of 5 molecules for 40−100 ps of transport down an 80 Å-long nanotube. Additionally, the ND I lines in Figure 3 are exclusively fit to data from the first stage to more fully understand molecular transport in this stage and to differentiate it from those of the other stages. However the ND II lines were obtained for transport through the entire nanotube and were not broken down into stages. Therefore, the diffusion coefficients, which are proportional to the interceptions on the $\langle z^2 \rangle$ axis, are necessarily larger for ND I than those for ND II, because there is little interaction to inhibit the forward flow of methane molecules in the first stage.

Molecular transport can generally be described using the following expression:

$$\langle z^2 \rangle \sim t^{\alpha} \quad (6)$$

where the exponent, α, has different values, depending on the nature of the transport. In particular, $\alpha = 0.5$ for single-file motion, $1 < \alpha < 0.5$ is for inhibited diffusion, which is also known as subdiffusion, $\alpha = 1$ for Fickian or normal-mode diffusion, as shown in eq 4, $2 < \alpha < 1$ for accelerated diffusion, which is also called super-diffusion, or $\alpha \geq 2$ for ballistic motion.[51,52]

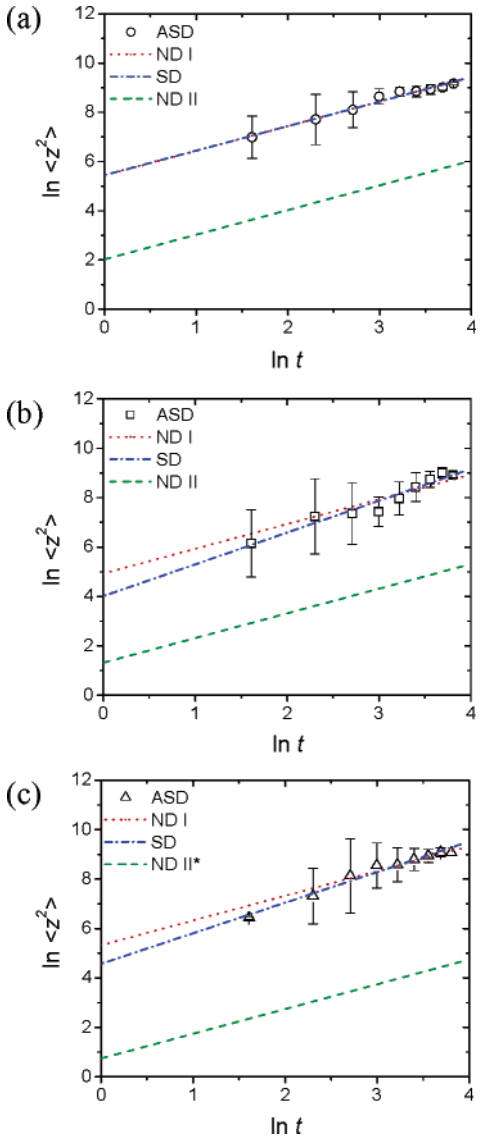

Figure 3. Log−log plots of average square displacement versus time of CH_4 molecules entering (a) (10,0), (b) (14,0), and (c) (17,0) nanotubes at the beginning of simulations (stage one). Explanation of the caption is provided in the text. *Means that the ND II line is fit to diffusion coefficients for CH_4@(16,0).

Superdiffusion has been observed under various conditions in many physical circumstances such as chaotic advection.[53] Recently, it was found in equilibrium molecular dynamics simulations that normal- and isopentane molecules show super-diffusion behavior when they flow through an opened (10,10) carbon nanotube, and several arguments were proposed to explain this behavior, including changes in levitation, conformation, and potential energy.[19] In equilibrium MD simulations at various temperatures,[54] the mean square displacements of methane molecules in about 1 μm-long and 0.5 μm-long (6,6) nanotubes progress through different transport modes, including from ballistic motion (at about 4 ps), normal, or single-file mode diffusion (at about 40 ps to 800 ps), and superdiffusion behavior (at about 0.8 to 1.2 μs). Supple et al.[55] also predict ballistic motion in a system of decane molecular flow through a rigid (13,13) nanotube, where the fast molecular transport is attributed

to the high driving force of convection. Subdiffusion and superdiffusion are known to occur when the molecular velocity does not vary finitely or the autocorrelation function of the Lagrangian velocities does not decay quickly enough.[56]

Line SD in Figure 3a, which is fit to the simulation data and used to extract the exponent, α, in eq 6, is coincident with line ND I; that is, the transport of methane molecules through the (10,0) nanotube is normal-mode in the first stage. Line SDs in Figures 3b and 3c show that the transport of methane through the (14,0) and (17,0) nanotubes possibly occurs via anomalous motion with $\alpha = 1.29$, and $\alpha = 1.24$, respectively. This is not surprising considering the highly nonequilibrium nature of the molecular transport in this stage. However, line ND I in Figures 3b and 3c agree just as well as the SD fit within the error bars of the data.

Because of the chaotic nature of molecular motion in the second stage, it is difficult to characterize transport. However, when region B is saturated with methane molecules, the gas density through the whole nanotube volume levels off and the material balance of one molecule leaving the nanotube as each new molecule enters is achieved in the third stage. The discontinuous molecular distribution and the frequent bouncing motion of the methane molecules make it difficult to quantify the density gradient through region B at any given instant. For gas molecules to continuously leave the nanotube, molecules need to keep entering the nanotube from region A. This means that the interactions between molecules in region A affect molecular passage through the carbon nanotube.

Figure 4 shows plots of log $\langle z^2 \rangle$ versus log t of CH_4 molecules that enter the (10,0), (14,0), and (17,0) zigzag nanotubes at different times after 200 ps of simulation time. Again, comparable behavior was seen for the similarly sized armchair (6,6), (8,8), and (10,10) nanotubes. In the case of the (10,0) nanotube shown in Figure 4a, ND I ($A = 1.116 \times 10^{-3}$ cm^2/s) does not fit the data well, and ND II fits just to data in the first half-time of the period. In contrast, the SD line ($\alpha = 1.62$) fits all the data very well. When we extended this simulation beyond 250 ps by adding more molecules to the reservoir (region A) and allowed the simulation to continue under near-equilibrium conditions, the SD line with $\alpha = 1.62$ reproducibly fit the simulation data. This indicates that the molecular transport does not follow either normal-mode diffusion or ballistic motion. In contrast, the molecular transport data for the (14,0) and (17,0) nanotubes shown in Figures 4b and 4c are fit well by the ND I lines, indicating that the molecules in these nanotubes follow normal-mode diffusion in agreement with previous findings[43,44,50] even as the data deviate further from the ND II lines. The reasons for the differences between the ND I and ND II fits are the same as those mentioned above for the first stage.

Thus, anomalous molecular transport continues for much longer times and under near-steady-state conditions in the smallest diameter (10,0) and (6,6) nanotubes whereas it proceeds via normal-mode diffusion for the larger (14,0), (17,0), (8,8) and (10,10) nanotubes. The exact corresponding exponents, α, and normal mode diffusion coefficients for all the nanotubes considered in this study are shown in Table 2. The predicted decrease of α as the size of the nanotube increases in stage 3 means that the anomalous transport behavior becomes less pronounced as the diameter of the nanotube increases. In other words, molecular transport approaches normal mode diffusion as the size of the nanotube increases. Previous findings[43,44,50] indicate that normal mode diffusion is dominant for methane molecular transport up to a pore size between 20 and 500 Å

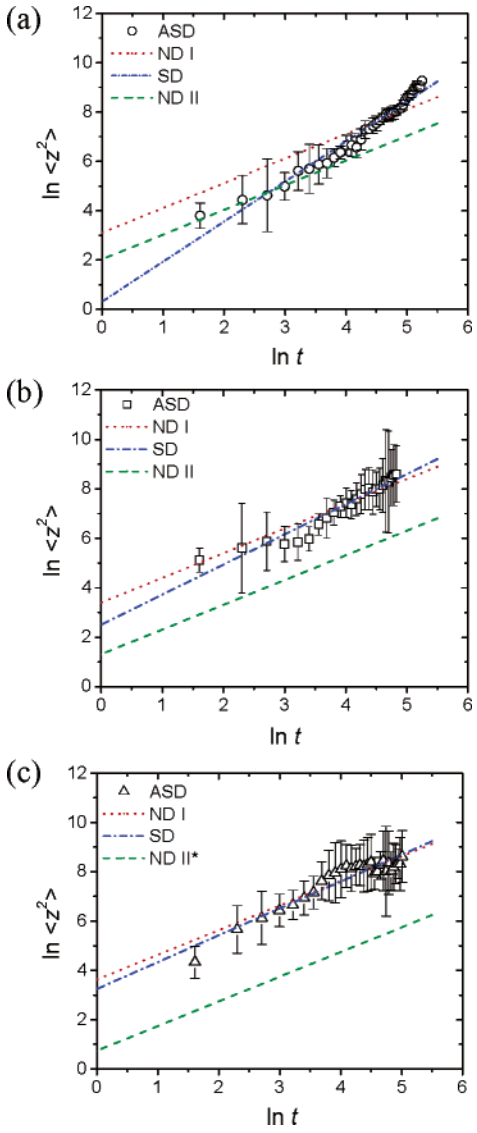

Figure 4. Log−log plots of average square displacement versus time of CH_4 molecules entering (a) (10,0), (b) (14,0), and (c) (17,0) nanotubes after 200 ps. *Means the ND II line is fit to diffusion coefficients for CH_4@(16,0).

TABLE 2: Exponents for Equation 6 and Normal Mode Diffusion Coefficients for Various Nanotubes

	stage 1		stage 3		
nanotube	α of SD	A of ND I (cm^2/s)	α of SD	A of ND I (cm^2/s)	A of ND II (cm^2/s)
10,0	1.00	1.149×10^{-2}	1.62	1.116×10^{-3}	3.80×10^{-4}
14,0	1.29	0.691×10^{-2}	1.22	1.498×10^{-3}	1.86×10^{-4}
17,0	1.23	1.025×10^{-2}	1.09	1.880×10^{-3}	
6,6	1.37	0.981×10^{-2}	1.62	0.828×10^{-3}	
8,8	1.85	1.100×10^{-2}	1.17	1.437×10^{-3}	1.86×10^{-4}
10,10	1.40	1.034×10^{-2}	1.20	2.394×10^{-3}	0.954×10^{-4}

where Knudsen diffusion becomes the predominant molecular transport mechanism.[57]

3.2. Why Anomalous Transport in the Smallest Diameter Nanotubes? There are several possible explanations for this continued anomalous behavior. One is that it represents a transition between normal mode diffusion and the ballistic convection of continuum theory.[58] While convection behavior is known to occur across gradients such as are present in the simulations, it is interesting that it is only predicted to occur in the smallest diameter nanotubes and not in the larger diameter tubes considered here. Additionally, conventional convection

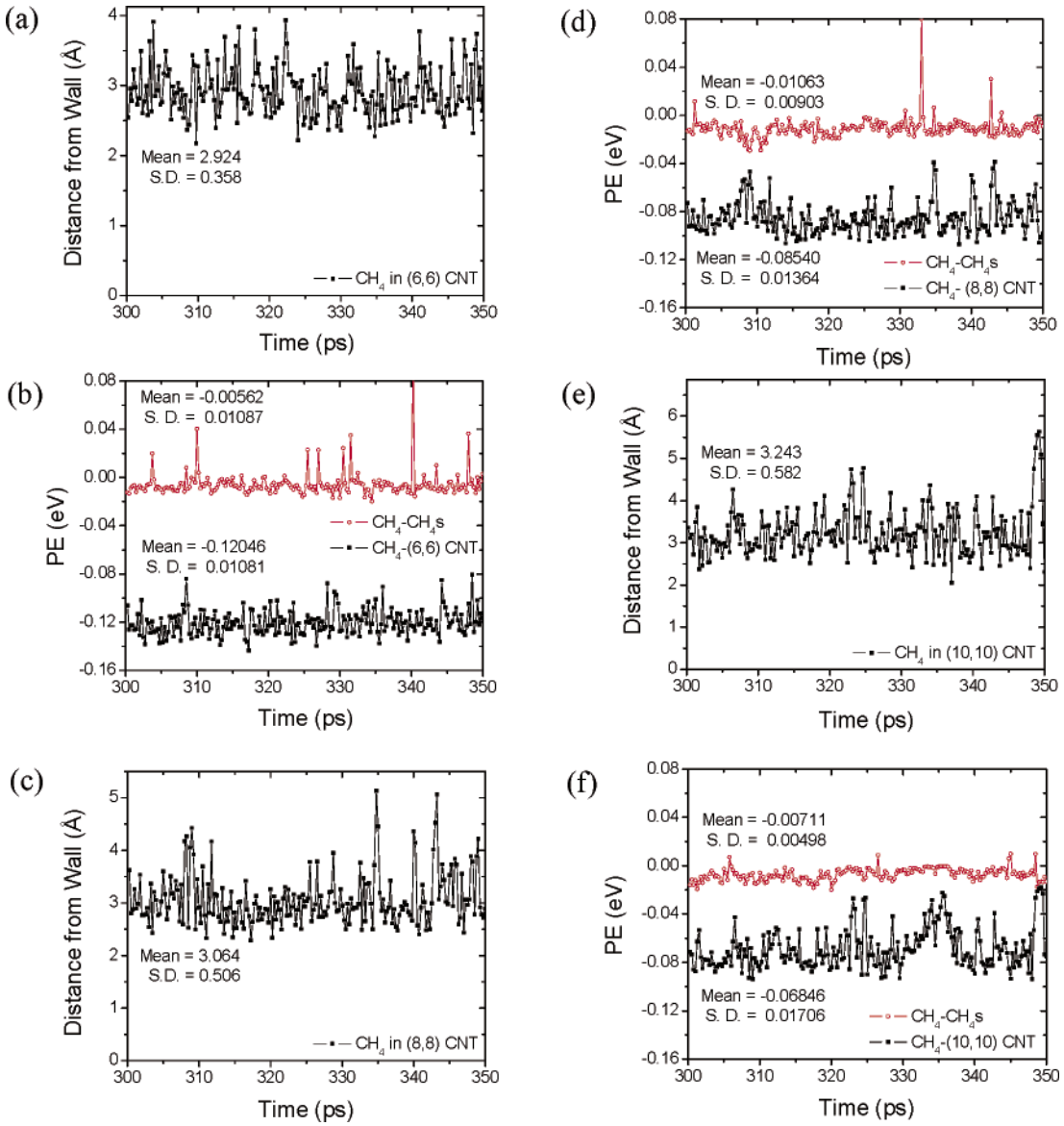

Figure 5. Variation of the distance between a CH_4 molecule and the walls of (a) (6,6), (c) (8,8), and (e) (10,10) nanotubes. The fluctuation of the potential energy between the CH_4 molecule and other CH_4 molecules (legend as CH_4-CH_4s) and between the CH_4 and the nanotubes (legends as CH_4-(n,n) CNT) in (b) (6,6), (d) (8,8), and (f) (10,10) nanotubes. S.D. denotes standard deviation.

theory cannot be used to explain the reverse motion of the methane molecules (from region C to region B) that occurs despite the pressure gradients in the systems. Last, it is possible that the larger diameter nanotubes reach near-steady-state conditions much more quickly than the smallest diameter nanotubes. In this case, the anomalous molecular transport in the smallest diameter nanotubes is merely indicative of the fact the system is still in transition and has residual ballistic molecular motion.

Bhide et al.[19] attributed their similar findings for the transport of pentane through single-walled carbon nanotubes, which they term superdiffusion, to a combination of nonballistic-diffusive (chaotic) motion in the radial direction and ballistic (regular) motion along the nanotube channel. Additionally, they find that velocity autocorrelation functions for the velocity components along the direction of the nanotube length do not decay, while the components along the orthogonal directions do decay. The conditions are somewhat different from the simulations reported here, however, in that in the simulations of Bhide et al., a single pentane molecule moves through the nanotube under equilibrium conditions without any pressure gradients.

Superdiffusion is normally associated with chaotic or obstacle-filled systems,[59] and its occurrence in nanopores with smooth walls such as carbon nanotubes is nonintuitive. To determine if in fact smooth nanotube walls can behave as an obstacle-filled system, the motion of one CH_4 molecule in three of the carbon nanotubes considered here is traced. In particular, the distance from the nanotube wall to the CH_4 being traced is plotted for the (6,6), (8,8), and (10,10) nanotubes in Figure 5. Figure 5 also shows how the potential energy surface of the CH_4 molecule being traced interacting with only the other CH_4 molecules in the nanotubes or only with the nanotubes themselves changes as a function of time for simulation times between 300 and 350 ps. Similar plots have been generated for other randomly chosen CH_4 "tracer" molecules and confirm that the results in Figure 5 are both reproducible and representative.

Figure 5a,c,e shows that the distance between the molecule and the nanotube wall changes frequently for all three nanotubes, which is an indication of molecular scattering, while the standard deviation increases with increases in the nanotube diameter. Figure 5b,d,f clearly shows that the interaction between the CH_4 molecule and the other CH_4 molecules in the nanotubes is more

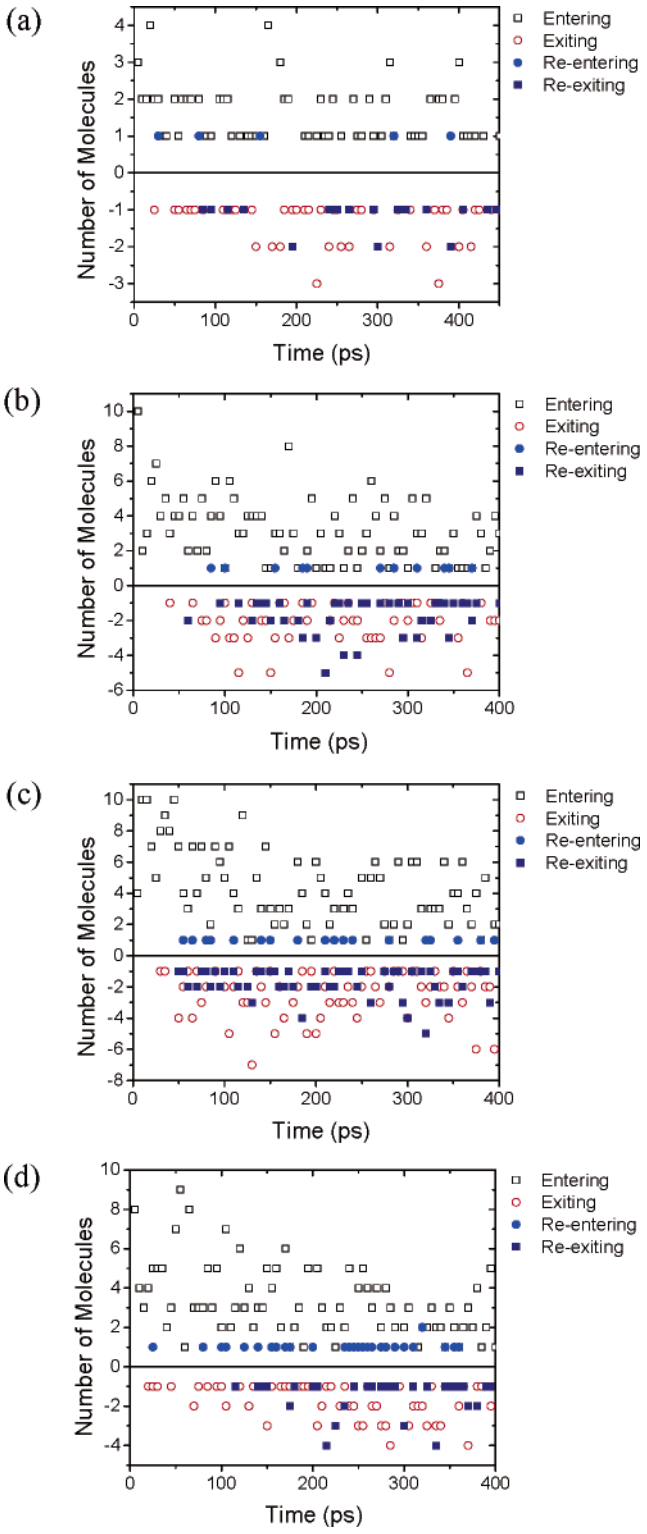

Figure 6. Plots of the number of molecules entering, exiting, re-entering, and re-exiting vs time for (a) (10,0), (b) (14,0), (c) (17,0), and (d) (10,10) nanotubes.

repulsive, and has more severe fluctuations, than the interaction between the CH_4 molecule and the nanotube wall. However, as the nanotube diameters increase, the repulsive character of the CH_4 interaction with other methane molecules decreases significantly, indicating fewer violent and elastic molecule−molecule collisions, while the fluctuation in the interaction of the CH_4 with the carbon nanotube increases, reflecting the more dispersed distribution of molecules throughout the larger nanotube interior.

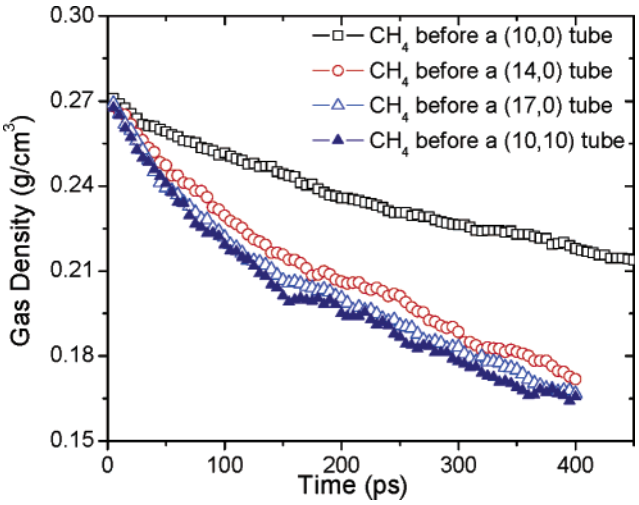

Figure 7. CH_4 density in the gas reservoir as a function of time for various nanotubes.

Significantly, the fluctuation in the CH_4−nanotube interaction for the smallest diameter (6,6) nanotube (estimated to be 0.02−0.04 eV, on average) is larger than both $^1/_2k_BT$ at 300 K (0.0125 eV) and the mean interaction of one CH_4 molecule with the other CH_4 molecules in the nanotube. Consequently, the scattering of the CH_4 molecules in the direction normal to the nanotube axis is strongly affected by the CH_4−nanotube interaction in a manner that is analogous to an obstacle-filled pore. However, as the nanotube diameter increases, the difference between the two sets of potential energy surfaces plotted in Figure 5b,d,f decreases and the dominant effect of the CH_4−nanotube interaction on scattering decreases. As a result, molecular transport through the nanotube approaches bulk normal-mode diffusion as the carbon nanotube diameters increase.

3.3. Characterization of Molecular Densities and Transport Paths. In Figure 6, the number of molecules that enter each nanotube from the gas reservoir (entering), the number of molecules that leave each nanotube for the posterior region (exiting), the number of molecules that re-enter the nanotube from the posterior region (re-entering), and the number of molecules which a nanotube repels back into the gas reservoir (re-exiting) are plotted for the (10,0), (14,0), (17,0), and (10,10) nanotubes. For clarity, the number of molecules that are exiting or re-exiting are represented with negative values. To avoid confusion from overlap of data points, data having a value of zero are not plotted. At about 30 ps, the first molecule leaves the nanotube and the third stage of transport is achieved. If graphs (a), (b), and (c) of Figure 6 are compared, it can be found that the number of re-exiting or re-entering molecules increases as the pore size increases. This is caused by a lower pressure of the gas reservoir. The gas reservoir of the (10,0) system is denser at any time than the other systems as shown in Figure 7, so its stronger interactions encourage the molecules to move forward.

Figure 7 shows how the CH_4 density changes in the gas reservoir (region A) as a function of time for different carbon nanotubes. The plots thus denote how quickly the CH_4 molecules can flow into the nanotube from the gas reservoir. As the diameter of the nanotubes decrease, the transport rate of CH_4 into the nanotube decreases. The plot indicates that the number of molecules in the gas reservoir decreases exponentially with time. Therefore the relationship between the number of molecules (or molecular density) in the reservoir and time can

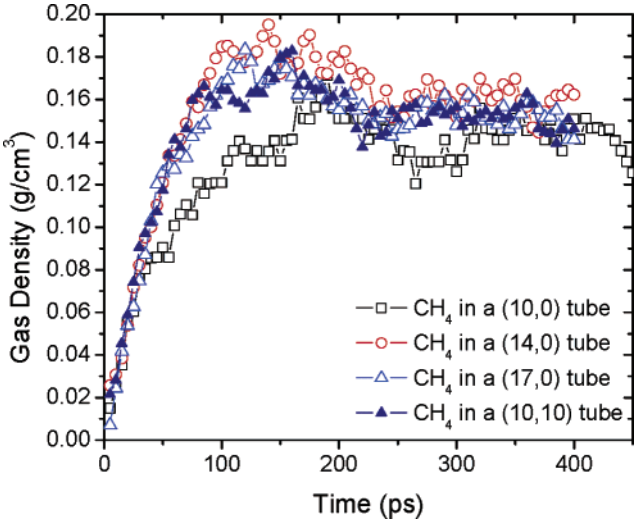

Figure 8. The CH_4 density changes in the nanotube region as a function of time for various nanotubes.

TABLE 3: Parameters for Equation 7 Fitted for Various Nanotubes

helicity	N_0/V (g/cm^3)	N_∞/V (g/cm^3)	a (ps^{-1})
10,0	0.273	0.150	0.0016
14,0	0.273	0.150	0.0040
17,0	0.273	0.150	0.0047
6,6	0.273	0.150	0.0020
8,8	0.273	0.150	0.0043
10,10	0.273	0.150	0.0051

be expressed as follows:

$$\frac{N}{V} = \frac{(N_0 - N_\infty)}{V} e^{-at} + \frac{N_\infty}{V} \tag{7}$$

where N is the number of gas molecules in the gas reservoir, subscripts 0 and ∞ indicate the values at the onset of transport and at infinite time, V is the volume of the reservoir, N/V is gas density, a is an index, and t is time. Because the volume of the reservoir is constant, the rate of transport of gas molecules into each carbon nanotube can be described as follows:

$$-\frac{1}{V}\frac{dN}{dt} = \frac{(N_0 - N_\infty)}{V} a e^{-at} = a\frac{(N - N_\infty)}{V} \tag{8}$$

That is, the transport rate depends on the density of gas in the reservoir. Since this density also can be described with gas pressure, the transport rate can be said to depend on the gas pressure of the reservoir. Table 3 shows the calculated values of N_0/V, N_∞/V, and a's by curve fitting for different nanotubes. The value of N_∞/V should be taken at very long times when the density levels off. However, in this case it was approximated as 0.15 g/cm^3 which is where the CH_4 density in the nanotubes increases (Figure 8). In the table, it is found that a is larger when the density decreases more rapidly. Therefore, this index a should indicate the amount of gas that can pass through each carbon nanotube. The relation of a to cross-sectional area and volume of various nanotubes is shown in Figure 9. According to the figure, a increases with the volume of the nanotube.

Figure 8 shows the plots of CH_4 density inside the carbon nanotubes (in region B) as a function of time for various carbon nanotubes. At times up to 30 ps, the gas densities increase with almost the same slope. This means that the number of entering molecules is proportional to the cross-sectional area of nanotube

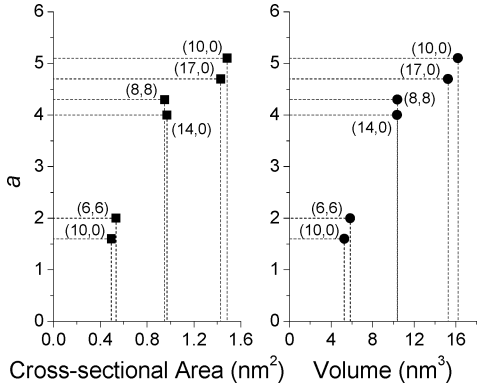

Figure 9. The dependence of the index a in eq 7 on the cross-sectional area and on the volume of various nanotubes.

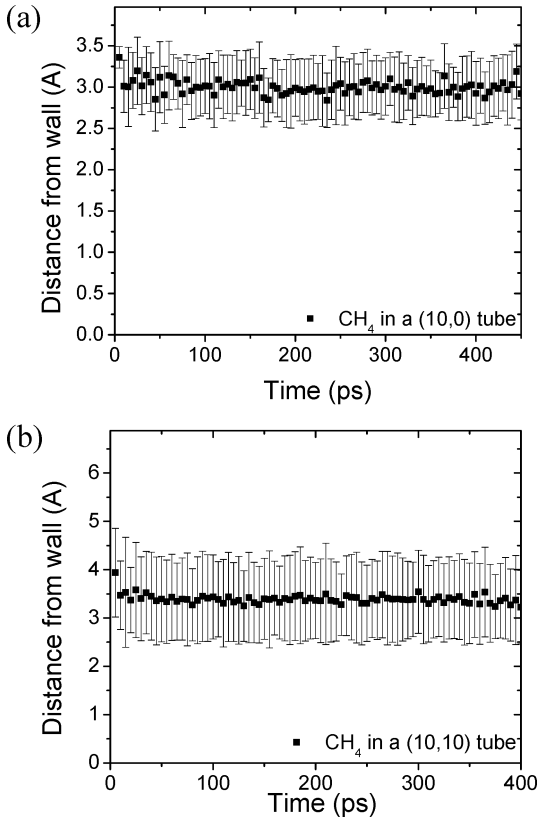

Figure 10. The distance between CH_4 molecules and the inner wall of nanotubes. (a) (10,0), and (b) (10,10) nanotubes.

pore in the first stage. After that, the CH_4 density in the tube region of the smallest nanotube increases more slowly than those of the larger nanotubes. This may seem to be discordant with the results of our previous research in which the diffusion coefficient of CH_4 decreases as the pore size of the nanotube increases.[43] However, these diffusion coefficients are taken from the displacements of gas molecules in region B only, and show that molecules can move faster in carbon nanotubes with smaller pore sizes than those that have larger pore sizes because the interactions between a methane molecule and the nanotube are getting stronger as the nanotubes pore size decreases. This finding is consistent with recent findings reported in ref 37. All the densities in Figure 8 level off at 200 ps to 300 ps, as the gas flow reaches steady-state in the carbon nanotubes. That is, the system has changed from a nonequilibrium state to an equilibrium state around 250 ps, even though there is still some fluctuation in densities. This is stage three. The molecular density in the gas reservoir decreases over this same time scale

and the steady-state molecular density in the carbon nanotubes (region B) can only be maintained by continually replenishing the gas reservoir (region A). Without this replenishment, the reservoir will ultimately be depleted as the majority of the molecules pass through the nanotube and into region C. The strong attractive interactions between the molecules and nanotube interior would keep the molecular density in the nanotubes at nonzero values, barring significant changes in conditions.

The diameters of (17,0) and (10,10) nanotubes are similar (see Table 1), but their helical structures are different from one another. From Figure 7 and Figure 8, it is clear that the difference in helicities of carbon nanotubes do not affect the CH_4 transport. This is in agreement with our previous findings.[43,44]

Figure 10 shows the distributions of methane molecules in the radial plane of two of the carbon nanotubes. The methane molecules prefer to be about 3 Å from the nanotube wall. As the diameter of the nanotube increases, this distance is slightly shifted to a longer value and the standard deviation increases. The distance depends on the integrated LJ potentials of the constituent atoms, and is comparable to the previously stated values, 2.56 Å for C−C, and at 2.86 Å for C−H, where the LJ potential is a minimum. This is why this result is different from the expectation that methane molecules are more stable when they are placed around the center of the nanotube interior rather than close to the inner wall.

4. Conclusions

The transport of spherical molecules of methane through smaller, single-walled nanotubes are considered in classical nonequilibrium molecular dynamics simulations. The results show that the rate of flow of the molecules does not depend on the helical symmetry of the carbon nanotube but does depend on the tube diameter. The number of gas molecules levels off when the molecules begin to pass out of the carbon nanotube and molecular bouncing at the ends of the tubes is reduced. In addition, the influx gas molecules prefer to stay a certain distance away from the nanotubes rather than moving along the center of the tube.

The results also indicate that the transport behavior can be broken down into three different consecutive stages with unique mechanisms. In the first stage, CH_4 molecules move down the nanotube with little interference from other CH_4 molecules. The molecular bouncing motion observed in the second stage when methane molecules are filling the carbon nanotubes is one characteristic of nonequilibrium transport and is caused by the small dimension of these systems. In particular, the dimensions of the molecules and the pore are comparable to the length corresponding to the minimum van der Waals interaction.

These results for nonequilibrium transport will help in the development of more realistic and reliable models for equilibrium transport. The CH_4 density in the nanotube increases and levels off at a saturation density, and then the transport behavior is transformed into that of the third stage where CH_4 molecules, with a small amount of bouncing motion, flow from the gas reservoir region to the posterior region in a linear manner. It is recognized that the time required to reach each of these stages will depend to a significant degree on the length of the carbon nanotube under consideration. These results should be compared with those from longer time simulations or of equilibrium transport to verify that equilibrium or near-equilibrium conditions are reached in the third stage.

Acknowledgment. The authors thank Zugang Mao for many helpful discussions and gratefully acknowledge the support of the NASA Ames Research Center and the NSF Supported Network for Computational Nanotechnology at Purdue University (EEC-0228390).

References and Notes

(1) de Vos, R. M.; Verweij, H. *Science* **1998**, *279*, 1710.
(2) Gergidis, L. N.; Theodorou, D. N. *J. Phys. Chem. B* **1999**, *103*, 3380.
(3) Mohanty, S.; McCormick, A. V. *Chem. Eng. J.* **1999**, *74*, 1.
(4) Thomson, K. T.; Wentzcovitch, R. M. *J. Chem. Phys.* **1998**, *108*, 8584.
(5) Keffer, D.; Davis, H. T.; McCormick, A. V. *J. Phys. Chem.* **1996**, *100*, 638.
(6) Skoulidas, A. I.; Sholl, D. S.; Krishna, R. *Langmuir* **2003**, *19*, 7977.
(7) Ayappa, K. G. *Langmuir* **1998**, *14*, 880.
(8) Khan, I. A.; Ayappa, K. G. *J. Chem. Phys.* **1998**, *109*, 4576.
(9) Nelson, P. H.; Auerbach, S. M. *J. Chem. Phys.* **1999**, *110*, 9235.
(10) Levitt, D. G. *Phys. Rev. A* **1973**, *8*, 3050.
(11) Sholl, D. S.; Fichthorn, K. A. *J. Chem. Phys.* **1997**, *107*, 4384.
(12) Sholl, D. S. *Chem. Eng. J.* **1999**, *74*, 25.
(13) Keffer, D.; Mccormick, A. V.; Davis, H. T. *Mol. Phys.* **1996**, *87*, 367.
(14) Keffer, D.; McCormick, A. V.; Davis, H. T. *J. Phys. Chem.* **1996**, *100*, 967.
(15) Keffer, D.; Davis, H. T.; McCormick, A. V. *J. Int. Adsorption Soc.* **1996**, *2*, 9.
(16) Bennett, J. M.; Cohen, J. P.; Flanigen, E. M.; Pluth, J. J.; Smith, J. V. *ACS Symp. Ser.* **1983**, *218*, 109.
(17) Hahn, K.; Karger, J.; Kukla, V. *Phys. Rev. Lett.* **1996**, *76*, 2762.
(18) Gergidis, L. N.; Theodorou, D. N.; Jobic, H. *J. Phys. Chem. B* **2000**, *104*, 5541.
(19) Bhide, S. Y.; Yashonath, S. *J. Am. Chem. Soc.* **2003**, *125*, 7425
(20) Ackerman, D. M.; Skoulidas, A. I.; Sholl, D. S.; Karl Johnson, J. *Mol. Simul.* **2003**, *29*, 677.
(21) Ebbesen, T. W. *J. Phys. Chem. Solids* **1996**, *57*, 951.
(22) Eswaramoorthy, M.; Sen, R.; Rao, C. N. R. *Chem. Phys. Lett.* **1999**, *304*, 207.
(23) Ugarte, D.; Chatelain, A.; deHeer, W. A. *Science* **1996**, *274*, 1897.
(24) Pederson, M. R.; Broughton, J. Q. *Phys. Rev. Lett.* **1992**, *69*, 2689.
(25) Darkrim, F.; Levesque, D. *J. Chem. Phys.* **1998**, *109*, 4981.
(26) Wang, Q. Y.; Johnson, J. K. *J. Phys. Chem. B* **1999**, *103*, 4809.
(27) Wang, Q. Y.; Johnson, J. K. *J. Chem. Phys.* **1999**, *110*, 577.
(28) Tuzun, R. E.; Noid, D. W.; Sumpter, B. G.; Merkle, R. C. *Nanotechnology* **1996**, *7*, 241.
(29) Stan, G.; Bojan, M. J.; Curtarolo, S.; Gatica, S. M.; Cole, M. W. *Phys. Rev. B* **2000**, *62*, 2173.
(30) Stan, G.; Hartman, J. M.; Crespi, V. H.; Gatica, S. M.; Cole, M. W. *Phys. Rev. B* **2000**, *61*, 7288.
(31) Cole, M. W.; Crespi, V. H.; Stan, G.; Ebner, C.; Hartman, J. M.; Moroni, S.; Boninsegni, M. *Phys. Rev. Lett.* **2000**, *84*, 3883.
(32) Simonyan, V. V.; Diep, P.; Johnson, J. K. *J. Chem. Phys.* **1999**, *111*, 9778.
(33) Gatica, S. M.; Cole, M. W.; Stan, G.; Hartman, J. M.; Crespi, V. H. *Phys. Rev. B* **2000**, *62*, 9989.
(34) Yin, Y. F.; Mays, T.; McEnaney, B. *Langmuir* **1999**, *15*, 8714.
(35) Dillon, A. C.; Jones, K. M.; Bekkedahl, T. A.; Kiang, C. H.; Bethune, D. S.; Heben, M. J. *Nature* **1997**, *386*, 377.
(36) Ye, Y.; Ahn, C. C.; Witham, C.; Fultz, B.; Liu, J.; Rinzler, A. G.; Colbert, D.; Smith, K. A.; Smalley, R. E. *Appl. Phys. Lett.* **1999**, *74*, 2307.
(37) Skoulidas, A. I.; Ackerman, D. M.; Johnson, J. K.; Sholl, D. S. *Phys. Rev. Lett.* **2002**, *89*, 185901.
(38) Talapatra, S.; Zambano, A. Z.; Weber, S. E.; Migone, A. D. *Phys. Rev. Lett.* **2000**, *85*, 138.
(39) Muris, M.; Dufau, N.; Bienfait, M.; Dupont-Pavlovsky, N.; Grillet, Y.; Palmari, J. P. *Langmuir* **2000**, *16*, 7019.
(40) Hummer, G.; Rasaiah, J. C.; Noworyta, J. P. *Nature* **2001**, *414*, 188.
(41) Kalra, A.; Garde, S.; Hummer, G. *Proc. Natl. Acad. Sci. U.S.A.* **2003**, *100*, 10175.
(42) Bienfait, M.; Asmussen, B.; Johnson, M.; Zeppenfeld, P. *Surf. Sci.* **2000**, *460*, 243.
(43) Mao, Z. G.; Sinnott, S. B. *J. Phys. Chem. B* **2000**, *104*, 4618.
(44) Mao, Z. G.; Sinnott, S. B. *J. Phys. Chem. B* **2001**, *105*, 6916.
(45) Brenner, D. W.; Shenderova, O. A.; Harrison, J. A.; Stuart, S. J.; Ni, B.; Sinnott, S. B. *J. Phys.-Condens. Matter* **2002**, *14*, 783.
(46) Frenkel, D.; Smit, B. *Understanding Molecular Simulation*; Academic Press: San Diego, 1996.
(47) Allen, M. P.; Tildesley, D. J. *Computer Simulation of Liquids*; Clarendon: Oxford, 1987.
(48) NIST. Chemistry WebBook (http://webbook.nist.gov/chemistry/), 2003.

(49) Saito, R.; Fujita, M.; Dresselhaus, G.; Dresselhaus, M. S. *Appl. Phys. Lett.* **1992**, *60*, 2204.
(50) Sinnott, S. B.; Mao, Z. A.; Lee, K. H. *Comput. Model. Eng. Sci.* **2002**, *3*, 575.
(51) Shlesinger, M. F.; Klafter, J. *Phys. Rev. Lett.* **1985**, *54*, 2551.
(52) Gitterman, M. *Phys. Rev. E* **2000**, *62*, 6065.
(53) Zaslavsky, G. M. *Phys. Today* **1999**, *52*, 39.
(54) Sholl, D. S. Private Communication.
(55) Supple, S.; Quirke, N. *Phys. Rev. Lett.*, in press.
(56) Castiglione, P.; Mazzino, A.; Muratore-Ginanneschi, P.; Vulpiani, A. *Physica D: Nonlinear Phenomena* **1999**, *134*, 75.
(57) Malek, K.; Coppens, M.-O. *J. Chem. Phys.* **2003**, *119*, 2801.
(58) Tsukamoto, N.; Miyazaki, S.; Fujisaka, H. *Phys. Rev. E* **2003**, *67*, 016212.
(59) Li, B. W.; Wang, L.; Hu, B. B. *Phys. Rev. Lett.* **2002**, *88*, 223901.